(Received 24 December 2025, Accepted 12 January 2026, Scheduled 9 February 2026)

A Design Approach of High-Efficiency Filtering Power Amplifiers Using Harmonic-Tuned Network and Terminated Coupled-line Structures

Lang Ran, Bin Wang*, Yongxin Wang, and Shihao Chen

School of Electronic Science and Engineering, Chongqing University of Posts and Telecommunications, Chongqing, China

ABSTRACT: A design approach using a harmonic-tuned network (HTN) and terminated coupled-line structures (TCLSs) for high-efficiency filtering power amplifiers (FPA) is proposed in this paper, effectively addressing the efficiency degradation caused by the integration of filtering structures in conventional FPA designs. The proposed approach enables compact circuitry while providing bandpass filtering characteristics. Bandpass filtering is realized through the cascaded TCLSs, while the incorporation of open-circuit and short-circuit branches introduces additional transmission zeros and poles, significantly improving frequency selectivity. In addition, HTN enables precise control of the harmonic impedance, effectively improving the efficiency of the power amplifier (PA). Based on this approach, an FPA operating in the 2.3–2.6 GHz band is designed and implemented. Experimental results show that the FPA achieves a output power (Pout) of 40.8–41.3 dBm, a drain efficiency (DE) of 67.2–72.2%, a gain of 12.8–13.3 dB, and stopband suppression greater than 39 dB on both sides of the passband. These results verify the effectiveness of the proposed design in enhancing PA efficiency and enabling circuit miniaturization, while also providing a feasible design approach for FPA development.

1. INTRODUCTION

As one of the key components with the highest power consumption ratio in radio frequency front-end systems, the power and efficiency of the PA directly determine the performance of the entire system [1]. Class-F and Class-F^{-1} PAs, as well as continuous-mode PAs designed for bandwidth extension, have received considerable attention owing to their excellent efficiency characteristics [2–4]. The output stage of a PA typically requires cascaded bandpass filters to efficiently suppress out-of-band spurious components and to maintain spectral purity. In traditional design methodologies, the PA and the filter are implemented as separate modules. Such an architecture not only increases system size and insertion loss, but may also degrade overall performance [5]. To address these challenges, an innovative co-design approach that integrates the PA and filter, referred to as the FPA, has recently emerged [6]. By incorporating the filtering function into the output matching network (OMN) of the PA and directly connecting it to the transistor drain, this approach effectively reduced the interconnect mismatch and insertion loss. Consequently, both system performance and integration are significantly improved [7].

Various structures and approaches have been employed in current research on FPA designs. Architectures, such as hybrid cavity microstrip filters [8], substrate integrated waveguide [9], and three-dimensional high-Q resonators [10], have been employed in OMNs to achieve high selectivity. However, these designs still face significant limitations in terms of bandwidth extension and structural simplification. Microstrip circuits have gained increasing popularity in modern circuit design owing to their significant advantages, including low cost and easy integration and fabrication [11–16]. The asymmetric open coupled-line (CL) technique [11] enhances bandpass filtering while effectively suppressing second-harmonic components, thereby improving the overall efficiency. A microstrip hairpin bandpass filter [12] was employed in output matching circuits to achieve device miniaturization. Although the ring-topology coupled-line design in [13] achieves a 50% fractional bandwidth and a microstrip bandpass filter with open-circuited parallel stubs in [14] freely extends the bandwidth to approximately one octave by modifying the characteristic impedance, both approaches suffer from a pronounced efficiency degradation across the entire passband. An unequal-width-three-coupled line and a diode matrix in are employed [15] to realize high-selectivity filtering and tunable bandwidth. The TCLS [16] demonstrates notable effectiveness in balancing out-of-band suppression and bandwidth. However, it still faces technical challenges such as increased insertion loss, reduced efficiency, and limited power.

In this paper, a design approach for high-efficiency FPA operating over the 2.3–2.6 GHz (corresponding to 5G NR band n40 and n7) is presented by integrating HTN with cascaded TCLSs in an OMN. Compared with a single TCLS, the cascaded TCLSs provide bandpass filtering characteristics with enhanced stopband suppression, while open-circuited and short-circuited branches introduce additional transmission zeros and poles to improve frequency selectivity. HTN further enables precise control of the harmonic impedance, enabling

* Corresponding author: Bin Wang (wangbin1@cqupt.edu.cn).

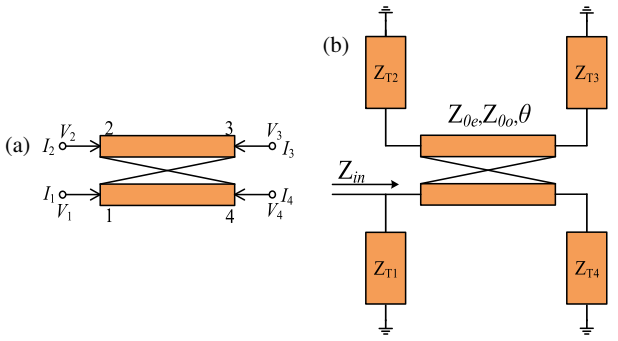

FIGURE 1. Schematic diagram of (a) traditional CL structure, (b) TCLS.

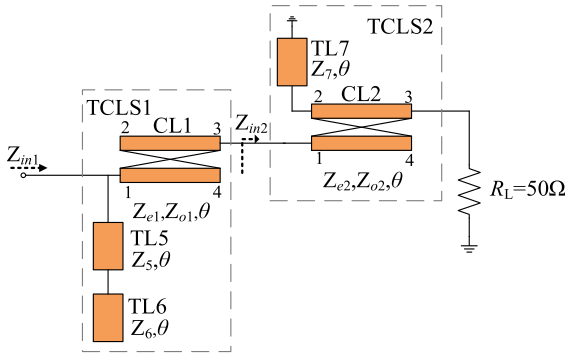

FIGURE 2. Schematic diagram of cascaded TCLS filter structure.

the PA to operate in a high-efficiency region. The measured DE ranges from 67.2% to 72.2%, with a Pout exceeding 40.8 dBm. The proposed design approach offers improved output performance and reduced circuit size, and is suitable for 5G transmitter front-ends.

2. THEORETICAL ANALYSIS

A conventional CL structure is shown in Figure 1(a). This structure is characterized by two primary parameters: even-mode impedance Z_{0e} and odd-mode impedance Z_{0o}. The voltages and currents at the four ports are denoted by V_i and $I_i\,(i = 1, 2, 3, 4)$. Based on the transmission line theory, the impedance matrix of the four-port network is given in (1).

$$\begin{bmatrix} V_1 \\ V_2 \\ V_3 \\ V_4 \end{bmatrix} = \begin{bmatrix} Z_{11} & Z_{12} & Z_{13} & Z_{14} \\ Z_{21} & Z_{22} & Z_{23} & Z_{24} \\ Z_{31} & Z_{32} & Z_{33} & Z_{34} \\ Z_{41} & Z_{42} & Z_{43} & Z_{44} \end{bmatrix} \cdot \begin{bmatrix} I_1 \\ I_2 \\ I_3 \\ I_4 \end{bmatrix} \tag{1}$$

$$Z_1 = Z_{11} = Z_{22} = Z_{33} = Z_{44} = -j\frac{Z_{0e} + Z_{0o}}{2\tan\theta} \tag{2}$$

$$Z_2 = Z_{12} = Z_{21} = Z_{34} = Z_{43} = -j\frac{Z_{0e} - Z_{0o}}{2\tan\theta} \tag{3}$$

$$Z_3 = Z_{13} = Z_{31} = Z_{24} = Z_{42} = -j\frac{Z_{0e} - Z_{0o}}{2\sin\theta} \tag{4}$$

$$Z_4 = Z_{14} = Z_{41} = Z_{23} = Z_{32} = -j\frac{Z_{0e} + Z_{0o}}{2\sin\theta} \tag{5}$$

A TCLS based on a conventional CL structure is shown in Figure 1(b). The parameters Z_{T1}, Z_{T2}, Z_{T3}, and Z_{T4} denote the terminal impedances connected to the four ports, whereas the overall input impedance of the structure, represented by Z_{in}, is given in (6).

$$Z_{in} = \frac{Z_{T1}\left(Z_1Q + Z_2M + Z_3N + Z_4P\right)}{Z_{T1}Q + Z_1Q + Z_2M + Z_3N + Z_4P} \tag{6}$$

where

$$\begin{aligned} M &= \left(Z_2Z_4 - Z_3(Z_1 + Z_{T3})\right)\left(Z_3Z_4 - Z_2(Z_1 + Z_{T4})\right) \\ &\quad + \left(Z_3^2 - Z_2^2\right)\left(Z_2Z_3 - Z_4(Z_1 + Z_{T4})\right) \end{aligned} \tag{7}$$

$$\begin{aligned} N &= Z_3\left(Z_1Z_3 - Z_2Z_4\right)\left(Z_1 + Z_{T2} + Z_{T4}\right) \\ &\quad + Z_3\left(Z_2^2 - Z_3^2 + Z_4^2 + Z_{T2}Z_{T4} - Z_1Z_2Z_4\right) \end{aligned} \tag{8}$$

$$\begin{aligned} P &= Z_3\left(Z_1Z_4 - Z_2Z_3\right)\left(Z_1 + Z_{T2} + Z_{T3}\right) \\ &\quad + Z_4\left(Z_2^2 + Z_3^2 - Z_4^2 + Z_{T2}Z_{T3} - Z_1Z_2Z_3\right) \end{aligned} \tag{9}$$

$$\begin{aligned} Q &= \left(Z_2(Z_1 + Z_{T2}) - Z_3Z_4\right)\left(Z_2Z_3 - Z_4(Z_1 + Z_{T4})\right) \\ &\quad + \left(Z_3(Z_1 + Z_{T3}) - Z_2Z_4\right)\left(Z_3^2 - (Z_1 + Z_{T2})\right. \\ &\quad \left.(Z_1 + Z_{T4})\right) \end{aligned} \tag{10}$$

The circuit topology of the proposed filter is shown in Figure 2, where two cascaded TCLSs are employed to attain broadband characteristics, low insertion loss, and improved stopband suppression. The TCLS1 unit consists of two transmission lines, TL5 and TL6, and CL1, with ports 2 and 4 terminated in the open circuits. The TCLS2 unit comprises a CL2 structure and a short-circuit branch TL7, with port 4 configured as open-circuited. The even-mode and odd-mode impedances of each CL are denoted as Z_{ei} and Z_{oi} $(i = 1, 2)$, and the two CLs share the same electrical length. The characteristic impedance and electrical length of the transmission lines are denoted by Z_i $(i = 5, 6, 7)$ and θ, respectively.

For TCLS1 and TCLS2, the design port impedances are specified in (11) and (12), respectively.

$$\begin{aligned} Z_{T1} &= jZ_5\frac{\tan\theta - k\cot\theta}{1 + k},\ Z_{T2} = \infty, \\ Z_{T3} &= Z_{in2},\ Z_{T4} = \infty \end{aligned} \tag{11}$$

where $k = Z_6/Z_5$.

$$Z_{T1} = \infty,\ Z_{T2} = jZ_7\tan\theta,\ Z_{T3} = 50\,\Omega,\ Z_{T4} = \infty \tag{12}$$

When the impedance transformation ratio is specified as $R = R_L/Z_{in} = 5$, the required input impedance is determined using the impedance transformation equation corresponding to the filter topology, thereby satisfying the desired impedance-matching requirements. The resulting design parameters were as follows in Table 1.

As shown in Figure 3, the transmission characteristics of the designed filter were significantly influenced by the configurations of TL5, TL6, and TL7. TL5 and TL6 are responsible for generating two transmission zeros (f_{Z2} and f_{Z3}) within the filter response, as derived analytically in (16).

TL3 generates two transmission poles, further enhancing the frequency selectivity. This structure effectively enhanced the

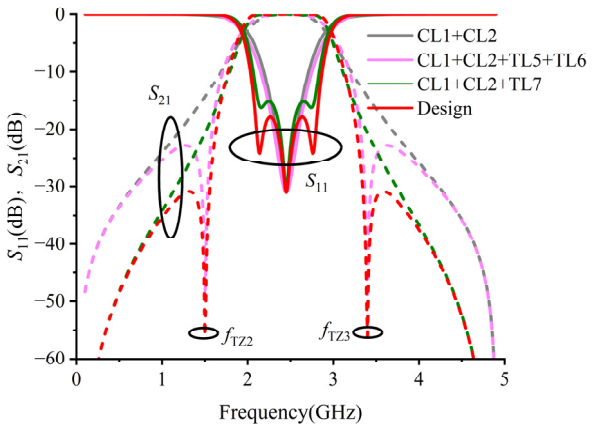

FIGURE 3. Effect of different transmission lines on filter S-parameters.

	Z (Ω)	Z_e (Ω)	Z_o (Ω)	θ (°)
TL5	34	N/A	N/A	90
TL6	70.6	N/A	N/A	90
TL7	30	N/A	N/A	90
CL1	N/A	66.7	38	90
CL2	N/A	101	35	90

TABLE 1. Designed filter parameters.

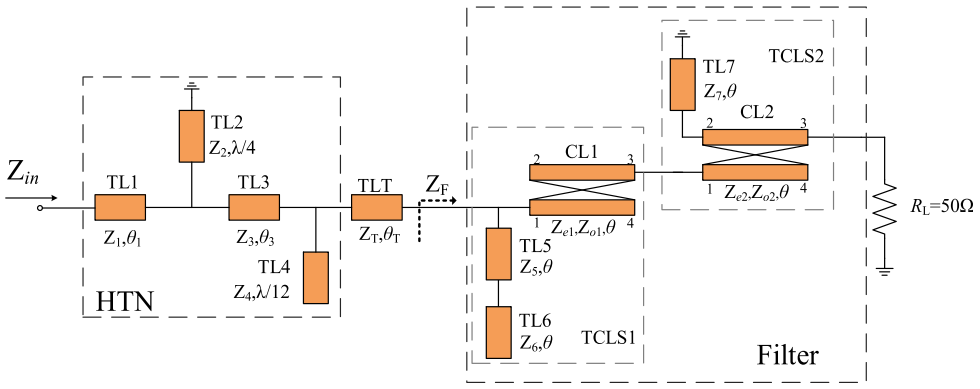

FIGURE 4. Schematic diagram of filtering OMN.

frequency selectivity. Moreover, because all electrical lengths were 90°, the introduction of TL5, TL6, and TL7 caused negligible disturbance to the center-frequency matching.

$$Z_{in} = 0 \Rightarrow Z_{T1} = 0 \Rightarrow \tan\theta - k\cot\theta = 0 \tag{13}$$

$$\begin{cases} \theta = \arctan\sqrt{k} \\ \theta = \pi - \arctan\sqrt{k} \end{cases} \tag{14}$$

where θ is

$$\theta = \beta l = \frac{2\pi}{\frac{c}{f_{TZ}}}\frac{\frac{c}{f_0}}{4} = \frac{\pi}{2}\frac{f_{TZ}}{f_0} \tag{15}$$

$$\begin{cases} f_{Z2} = \frac{2f_0}{\pi}\arctan\sqrt{k} \\ f_{Z3} = 2f_0 - \frac{2f_0}{\pi}\arctan\sqrt{k} \end{cases} \tag{16}$$

The structure of the proposed filtering OMN is shown in Figure 4. This configuration comprises an HTN and a filtering circuit. The cascaded TCLS network can achieve partial impedance transformation, but it cannot match the imaginary part impedance. This limitation may reduce Pout, thus affecting the normal operation of PA. To improve the efficiency, an HTN is integrated before the filter. The $\lambda/4$ transmission line TL2 generates a short-circuit condition for the second harmonic, while maintaining the matching of the third harmonic.

The impedance of the second harmonic is represented as

$$Z(2f_0) = R_2 + j * X_2 \tag{17}$$

Generally, R_2 is negligible and assumed to be zero. Accurate impedance matching of the imaginary component of the second harmonic is accomplished using the transmission line TL1, as expressed in (18).

$$\theta_1 = \frac{1}{2}\arctan\left(\frac{X_2}{Z_1}\right) \tag{18}$$

Consequently, the $\lambda/12$ open-line TL4 generates a short-circuit condition for the third harmonic. Through TL1 and transmission line TL3, the third harmonic impedance approaches an open-circuit condition because the electrical lengths of these two lines satisfy

$$\theta_3 = \lambda/12 - \theta_1 \tag{19}$$

TABLE 2. Load pull and source impedance.

Frequency (GHz)	2.3	2.45	2.6
Z_{fund} (Ω)	14.2+j*10.1	13.6+j*11.1	10.9+j*9.6
Z_{second} (Ω)	0.3+j*18.5	0.3+j*18.3	0.3+j*18.1
Z_{source} (Ω)	6.1−j*4.0	6.1−j*3.8	6.3−j*5.3

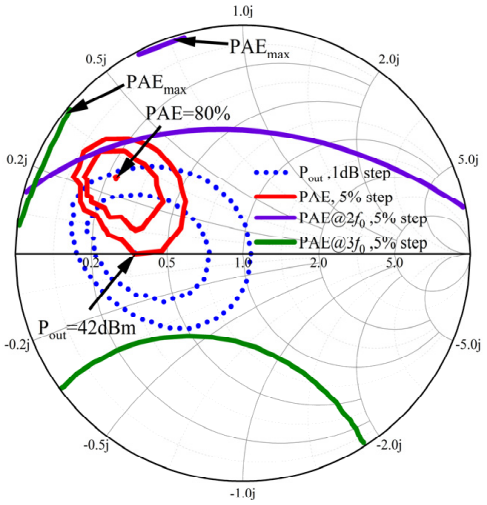

FIGURE 5. High-performance impedance area.

	$Z\ (\Omega)$	$Z_e\ (\Omega)$	$Z_o\ (\Omega)$	$\theta\ (^\circ)$
TL1	28.2	N/A	N/A	16.9
TL2	50	N/A	N/A	90
TL3	28.2	N/A	N/A	12.8
TL4	24.5	N/A	N/A	30
TLT	24.5	N/A	N/A	5.2
TL5	31	N/A	N/A	90
TL6	76.5	N/A	N/A	90
TL7	33.5	N/A	N/A	90
CL1	N/A	66.5	37.5	90
CL2	N/A	97	33	90

TABLE 3. Design parameters of the filtering OMN.

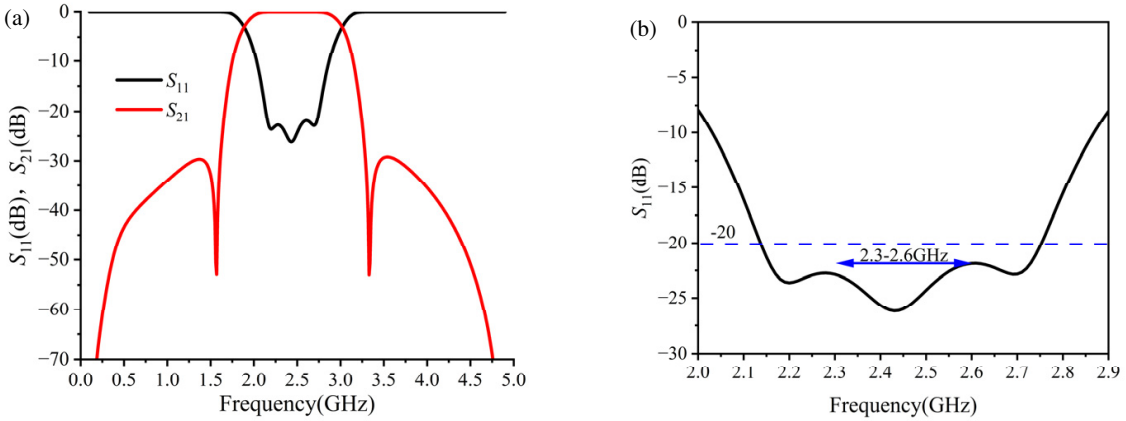

FIGURE 6. (a) S-parameter simulation results for the filter output matching. (b) Magnified view of S_{11} simulation result.

Additionally, a tuning line (TLT) is introduced between the HTN and the filter to convert the complex impedance at the fundamental frequency into the real part impedance. This adjustment facilitates favorable impedance matching at the filter input.

3. DESIGN OF THE PROPOSED FPA

The proposed FPA operates within the 2.3–2.6 GHz, centered at 2.45 GHz. A 10 W GaN transistor CGH40010F was selected as the core device, with the gate and drain bias voltages set to -2.8 V and 28 V respectively. The high-performance impedance area achieved through the load-pull and source-pull technologies are shown in Figure 5. The fundamental and second-harmonic impedances of the transistors are summarized in Table 2. The extracted fundamental impedance within the transistor operating frequency band is $Z(f_0) = 13.6+\text{j}*11.1\ \Omega$. HTN was designed according to (17)–(19). The TLT was employed to adjust the fundamental complex impedance to 11 Ω. The HTN design and filter parameters are presented in Table 3. The S-parameter response of the designed filtering OMN, along with the fundamental and harmonic impedance trajectories, are presented in Figures 6 and 7.

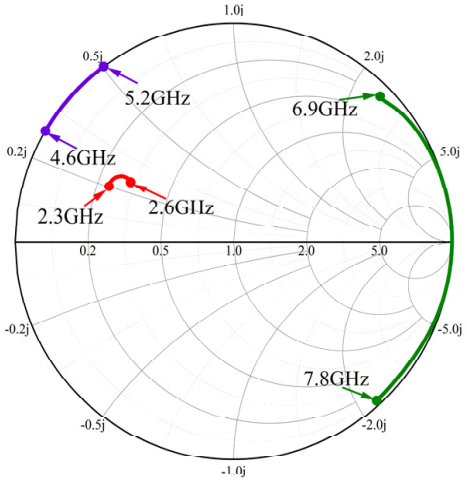

FIGURE 7. Fundamental and second- and third-harmonic impedance trajectories.

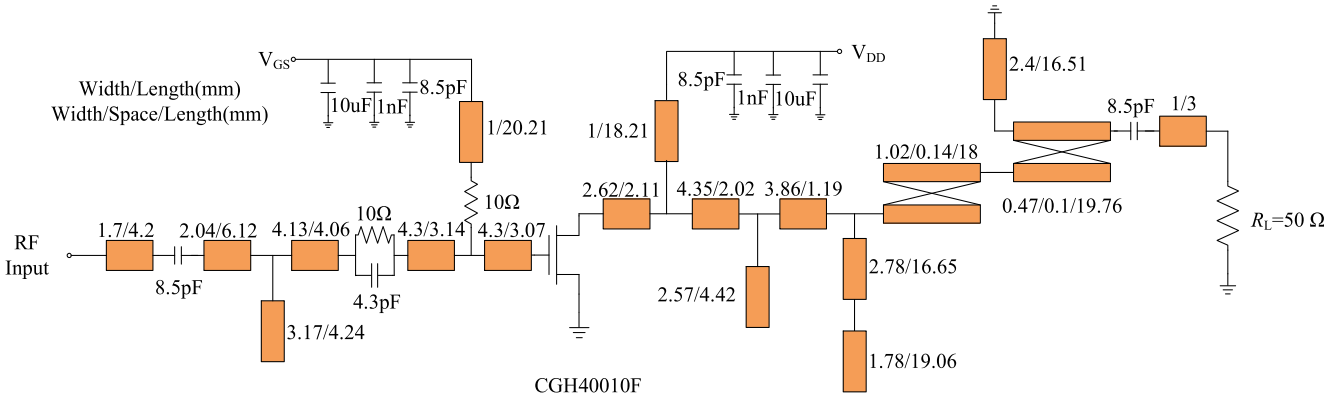

FIGURE 8. Schematic diagram of the proposed FPA structure.

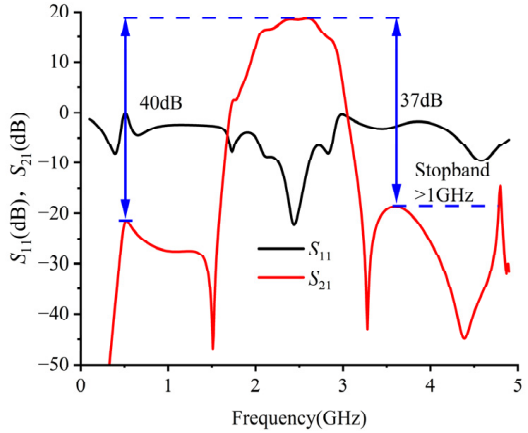

FIGURE 9. S-parameters of the filter amplifier designed for simulation.

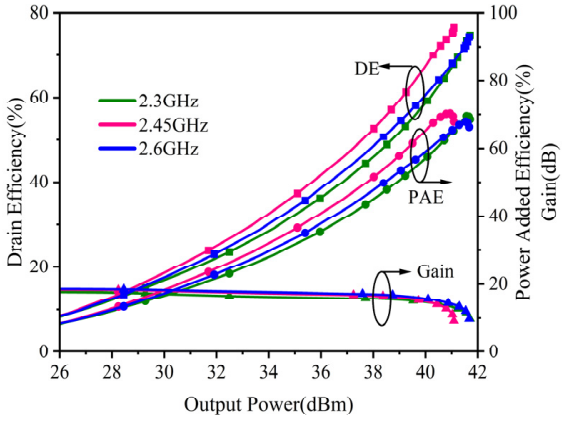

FIGURE 10. Simulated DE, PAE, and gain of the proposed FPA with Pout.

As shown in Figure 6, within the 2.3–2.6 GHz, $S_{11} < -20$ dB, indicating that accurate fundamental impedance matching was achieved through the tuning line and filter. In addition, the proposed circuit exhibited pronounced bandpass filtering characteristics and excellent stopband suppression.

As illustrated in Figure 7, the HTN structure realizes precise second-harmonic matching while simultaneously directing the third harmonic toward the high-efficiency operating region near the open circuit point.

An FPA is designed using the topology shown in Figure 8 to validate the effectiveness of the proposed filtering output matching circuit. The circuit was implemented on a ROGERS 4350B substrate with a relative permittivity $\varepsilon_r = 3.66$ and a thickness of 0.508 mm. To improve PA stability and suppress low-frequency oscillations, a stabilization network consisting of a 10 Ω resistor in parallel with a 4.3 pF capacitor was incorporated. In addition, a 10 Ω resistor was inserted in series at the gate to further enhance stability. The circuit S-parameter simulation results obtained from the ADS are shown in Figure 9. Within the 2.3–2.6 GHz band, the gain remains relatively stable and ranges from 17.8 to 18.5 dB. The value of S_{11} remains below −10.4 dB, confirming favorable input-matching characteristics while demonstrating excellent in-band flatness and desirable bandpass filtering performance.

Notably, the introduction of additional transmission zeros significantly enhances the frequency selectivity of this topology. Both the upper and lower stopband attenuations exceeded 37 dB, with stopband bandwidths exceeding 1 GHz.

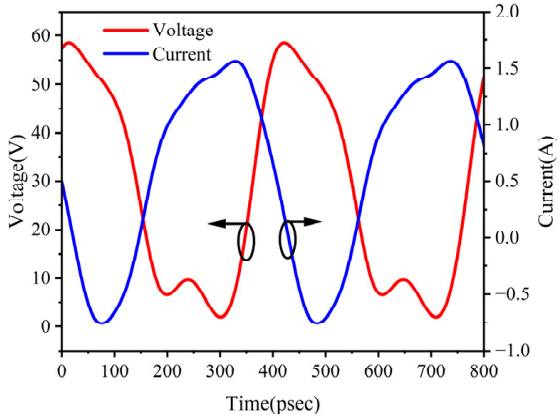

FIGURE 11. Drain voltage and current waveforms at 2.45 GHz.

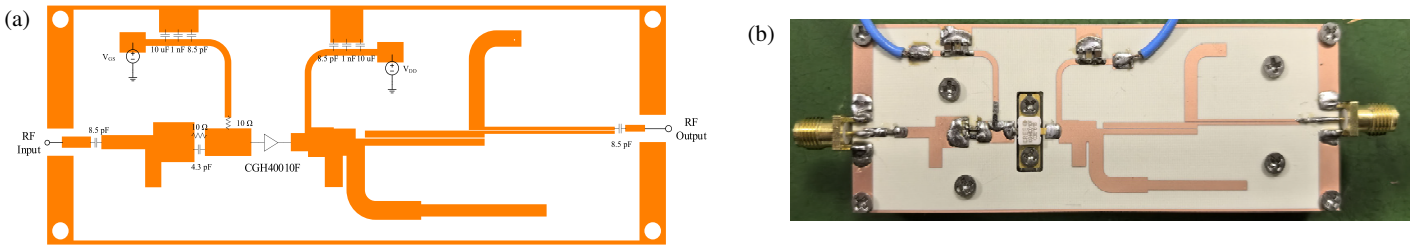

FIGURE 12. (a) Layout diagram. (b) Photograph of the fabricated FPA.

TABLE 4. Performance comparison with recently published FPAs.

Reference	Frequency (GHz)	Pout (dBm)	Gain (dB)	Efficiency (%)	Size ($\lambda_g * \lambda_g$)
2020 [16]	2.0–2.4	39–40.4	10.6	69–78.2^{D}	$1.11 * 0.61$
2020 [17]	3.3–3.6	40.4–40.6	8.6–10.8	62.3–68.9^{D}	$1.54 * 0.79$
2020 [18]	2	40.5	12	62^{P}	$1.06 * 0.56$
2022 [19]	3.3–3.7	39.5–41.6	9.7–11.5	58.8–72^{D}	$1.57 * 0.78$
2023 [20]	3.3–3.8	38.8–41.5	12.7–13.5	62.4–71.7^{P}	N/A
2023 [21]	1.85–2.1	38.6–39	8.9–10.2	58.5–73^{D}	$1.32 * 0.39$
2024 [22]	2.9–3.7	401–41.2	1–11.2	374–59.6^{D}	$1.1 * 0.85$
2025 [23]	2.2–2.9	39.6–41.6	8.6–10.8	61.6–73.7^{D}	$1.59 * 0.50$
2025 [24]	205–2.7	387–42	87–12	60.5–741^{D}	N/A
This work	2.3–2.6	40.8–41.3	12.8–13.3	67.2–72.2^{D}	$1.29 * 0.48$

D: drain efficiency, P: power added efficiency.

The large signal simulation results of DE, power added efficiency (PAE), and gain vary with Pout in the operating frequency band, as shown in Figure 10. The maximum Pout was 41.8 dBm, and the corresponding DE was 76.4%. At the same time, the peak PAE was 70.2%, and the gain was more than 12.4 dB. The drain voltage and current waveforms at 2.45 GHz are shown in Figure 11. The operating characteristics of the proposed FPA closely resemble those of a Class-F PA, as evidenced by the minimal overlap between the voltage and current within one cycle, which contributes to its high efficiency.

4. MEASUREMENT OF THE PROPOSED FPA

The fabricated FPA is shown in Figure 12, and the measured small-signal S-parameters obtained using an Agilent N5242A vector network analyzer are presented in Figure 13. Within the 2.3–2.6 GHz operating band, the measured small-signal gain ranges from 14.9 dB to 15.7 dB, exhibiting a 2.8 dB reduction compared with the simulated results. The discrepancy between the simulated and measured gains can be mainly attributed to several practical sources. The accuracy of the transistor nonlinear model is limited, which may lead to higher gain performance in the simulation. The model bias may affect the impedance matching effect, as shown in Figure 13(b), where S_{11} deteriorated from the simulated value of -22.3 dB to the measured value of -16.1 dB, thereby contributing to a reduction in the measured gain. In addition, fabrication tolerances of the microstrip lines, along with component soldering losses and possible thermal effects during measurement, further reduce the measured gain. The measured S_{11} remained below -10 dB across the passband. The upper and lower stopbands achieve suppression levels exceeding 39 dB, and the stopband bandwidth is greater than 1 GHz.

The measured DE, PAE, and gain results are shown in Figure 14. The maximum Pout is 41.7 dBm, corresponding to a DE of 73.4%, which is approximately 3% lower than the simulated value. A peak PAE of 68.1% was achieved and the measured gain exceeds 12.3 dB.

Within the 2.3–2.6 GHz band and under an input power of 28 dBm, the simulated and measured Pout, DE, and gain are shown in Figure 15. The measured Pout is 40.8–41.3 dBm, the DE is 67.2%–72.2%, and the gain is 12.8–13.3 dB, which is approximately 0.2 dB lower than the simulated value.

The performance of the designed FPA was summarized in Table 4 and compared with that of other published PAs. The FPA reported in [18] achieved a similar output performance comparable to that of this study and the proposed FPA operated over a broader bandwidth. Moreover, although the FPA in [16, 17, 19], and [21] exhibited comparable operating bandwidths, the PA developed in this study demonstrated superior performance in terms of key parameters, including Pout, DE, gain, and circuit size. Notably, while the FPA in [20] and [22–24] achieved bandwidths exceeding 500 MHz, the proposed FPA significantly improved the Pout flatness, maintained a high gain and efficiency, and further reduced the overall circuit size.

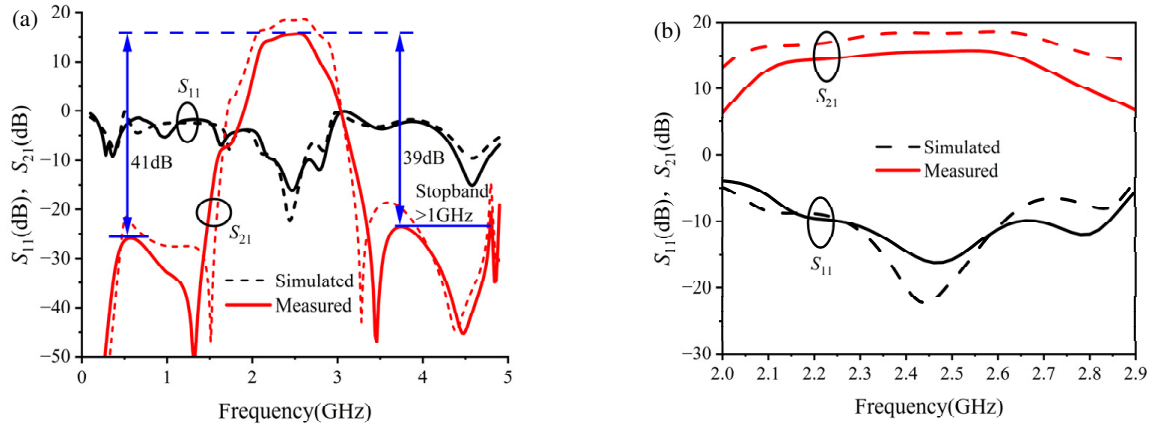

FIGURE 13. (a) Simulated and measured S-parameters of the proposed FPA. (b) Magnified view of the passband region.

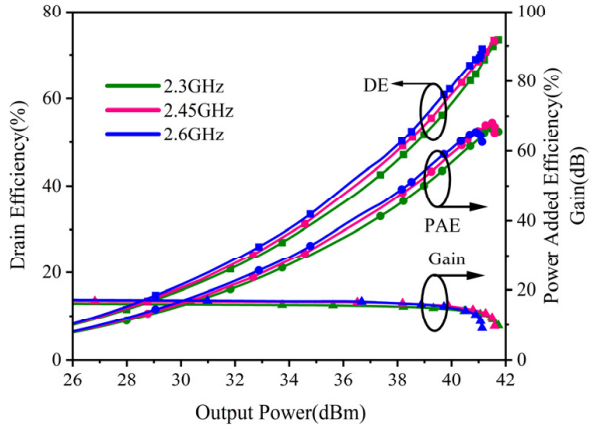

FIGURE 14. Measured DE, PAE, and gain of the proposed FPA with Pout.

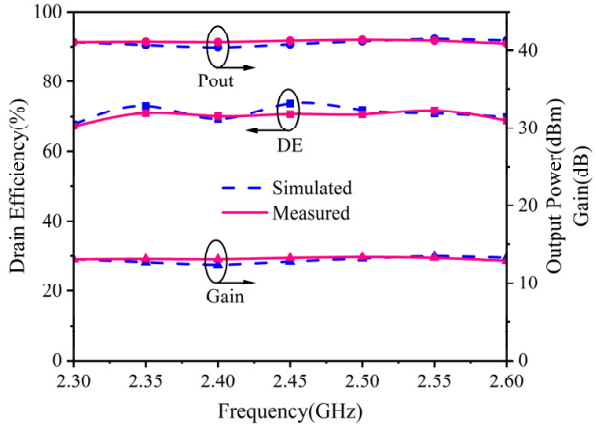

FIGURE 15. Simulated and measured Pout, DE, and gain of the proposed FPA with frequency.

5. CONCLUSION

This study presents an approach for designing a high-efficiency FPA by integrating HTN with TCLS. The TCLS not only provides bandpass filtering and enhanced stopband suppression but also introduces additional transmission zeros and poles to improve frequency selectivity through its open-circuit and short-circuit branches. HTN enables precise control of the harmonic impedance, resulting in improved PA efficiency. Together, these features enable a compact design with good bandpass performance, strong stopband suppression, and precise harmonic impedance control. Based on this approach, an FPA operating in the 2.3–2.6 GHz band is implemented. Measured results show that the FPA delivers a Pout of 40.8–41.3 dBm, a DE of 67.2%–72.2%, and stopband attenuation levels exceeding 39 dB on both sides of the passband. These results confirm the effectiveness of the proposed design approach in enhancing PA efficiency, improving frequency selectivity, and achieving circuit miniaturization, while also providing a viable approach for future FPA designs.

ACKNOWLEDGEMENT

This work was supported in part by the National Natural Science Foundation of China under Grant 62001074 and in part by the Chongqing Postgraduate Research and Innovation Project under Grant CYS21321.

REFERENCES

[1] Feng, T., K. Ma, Y. Wang, and J. Hu, "Bandpass-filtering power amplifier with compact size and wideband harmonic suppression," *IEEE Transactions on Microwave Theory and Techniques*, Vol. 70, No. 2, 1254–1268, 2022.

[2] Liu, C., "Analysis of class-F power amplifiers with a second-harmonic input voltage manipulation," *IEEE Transactions on Circuits and Systems II: Express Briefs*, Vol. 67, No. 2, 225–229, 2020.

[3] Ekhteraei, M., M. Hayati, and F. Shama, "High-efficiency low voltage inverse class-F power amplifier design based on harmonic control network analysis," *IEEE Transactions on Circuits and Systems I: Regular Papers*, Vol. 67, No. 3, 806–814, 2020.

[4] Nan, J., J. Yu, and H. Sun, "A design approach for high-efficiency hybrid continuous extended inverse class-F broadband power amplifier using band-pass network topology," *Progress In*

Electromagnetics Research M, Vol. 130, 129–137, 2024.

[5] Jian, Y., G. Liu, Z. Cheng, Z. Zhao, and W. Wang, "Compact broadband high-efficiency power amplifier using terminated coupled line filter matching network," *International Journal of RF and Microwave Computer-Aided Engineering*, Vol. 31, No. 11, e22815, 2021.

[6] Chen, K., J. Lee, W. J. Chappell, and D. Peroulis, "Co-design of highly efficient power amplifier and high-Q output bandpass filter," *IEEE Transactions on Microwave Theory and Techniques*, Vol. 61, No. 11, 3940–3950, 2013.

[7] Gao, Y., X. Shang, L. Li, C. Guo, and Y. Wang, "Integrated filter-amplifiers: A comprehensive review," *IEEE Microwave Magazine*, Vol. 23, No. 6, 57–75, 2022.

[8] Xu, J.-X., X. Y. Zhang, and X.-Q. Song, "High-efficiency filter-integrated class-F power amplifier based on dielectric resonator," *IEEE Microwave and Wireless Components Letters*, Vol. 27, No. 9, 827–829, 2017.

[9] Pech, P., P. Kim, and Y. Jeong, "Microwave amplifier with substrate integrated waveguide bandpass filter matching network," *IEEE Microwave and Wireless Components Letters*, Vol. 31, No. 4, 401–404, 2021.

[10] Gao, Y., W. Ma, D. Lu, B. Zhu, P. Jia, and M. Yu, "A coupling matrix synthesized three-dimensional filtering power amplifier," *IEEE Transactions on Circuits and Systems I: Regular Papers*, Vol. 71, No. 7, 3074–3085, 2024.

[11] Boumalkha, M., M. Lahsaini, M. E. H. Archidi, and Y. Achaoui, "Design of a wideband, highly efficient FPA using an asymmetrical open-circuit coupled-lines-based filtering matching network," *AEU — International Journal of Electronics and Communications*, Vol. 178, 155293, 2024.

[12] Haider, M. F., F. You, W. Shi, S. Ahmad, and T. Qi, "Broadband power amplifier using Hairpin bandpass filter matching network," *Electronics Letters*, Vol. 56, No. 4, 182–184, 2020.

[13] Boumalkha, M., M. Lahsaini, M. E. H. Archidi, M. F. Ghareeb, A. S. I. Amar, E. S. Oda, and S. F. Nafea, "Design of highly efficient filtering power amplifier with a wideband response for sub-6 GHz 5G applications," *Results in Engineering*, Vol. 24, 102905, 2024.

[14] Wang, W., H. Zhao, Y. Wu, and X. Chen, "5G wideband bandpass filtering power amplifiers based on a bandwidth-extended bandpass matching network," *China Communications*, Vol. 20, No. 11, 56–66, 2023.

[15] Pan, L., Y. Wu, W. Wang, S. Li, A. Piacibello, and V. Camarchia, "A broadband tunable high-selectivity bandpass filter and filtering power amplifier with continuous tunability and high stopband suppression level," *Microelectronics Journal*, Vol. 166, 106911, 2025.

[16] Su, Z., C. Yu, B. Tang, and Y. Liu, "Bandpass filtering power amplifier with extended band and high efficiency," *IEEE Microwave and Wireless Components Letters*, Vol. 30, No. 2, 181–184, 2020.

[17] Zhuang, Z., Y. Wu, M. Kong, and W. Wang, "High-selectivity single-ended/balanced DC-block filtering impedance transformer and its application on power amplifier," *IEEE Transactions on Circuits and Systems I: Regular Papers*, Vol. 67, No. 12, 4360–4369, 2020.

[18] Qi, X. and F. Xiao, "Filtering power amplifier with up to 4th harmonic suppression," *IEEE Access*, Vol. 8, 29 021–29 026, 2020.

[19] Jian, Y., G. Liu, and Z. Cheng, "Design of a broadband bandpass filtering power amplifier for 5G communication," *Microwave and Optical Technology Letters*, Vol. 64, No. 9, 1593–1599, 2022.

[20] Li, Y. C., R.-Z. Zhan, and Q. Xue, "Highly efficient filtering power amplifier using impedance area-based optimization," *IEEE Transactions on Circuits and Systems I: Regular Papers*, Vol. 70, No. 2, 556–565, 2023.

[21] Li, S., Y. Wu, Y. Yang, X. Chen, W. Wang, and Z. Chen, "Bandpass filtering power amplifier with wide stopband and high out-of-band rejection," *IEEE Transactions on Circuits and Systems II: Express Briefs*, Vol. 70, No. 3, 969–973, 2023.

[22] Liu, G., J. Yu, and Y. Lin, "Wideband filtering power amplifier based on terminated coupled line structure," *International Journal of Microwave and Wireless Technologies*, Vol. 16, No. 3, 418–423, 2024.

[23] Wang, K., Z. Cheng, M. Jia, Z. Zhu, B. Zhong, Z. Yang, and B. Li, "Design of a series of inverse continuous modes power amplifier based on bandpass filter," *International Journal of Circuit Theory and Applications*, Vol. 53, No. 7, 3949–3955, 2025.

[24] Zhong, B., Z. Cheng, M. Jia, B. Li, K. Wang, Z. Yang, and Z. Zhu, "Design of bandpass filtering power amplifier based on coupled microstrip line structure," *IEICE Transactions on Electronics*, Vol. E108-C, No. 5, 237–244, 2025.